

Document downloaded from:

<http://hdl.handle.net/10251/144808>

This paper must be cited as:

Rodríguez-Rodríguez, H.; Acebrón, M.; Iborra, F.; Arias-Gonzalez, JR.; Juárez, B. (25-0). Photoluminescence Activation of Organic Dyes via Optically Trapped Quantum Dots. ACS Nano. 13(6):7223-7230. <https://doi.org/10.1021/acsnano.9b02835>



The final publication is available at

<https://doi.org/10.1021/acsnano.9b02835>

Copyright American Chemical Society

Additional Information

This document is the Accepted Manuscript version of a Published Work that appeared in final form in ACS Nano, copyright © American Chemical Society after peer review and technical editing by the publisher.

# Photoluminescence Activation of Organic Dyes *via* Optically Trapped Quantum Dots

*Héctor Rodríguez-Rodríguez<sup>2</sup> María Acebrón,<sup>1</sup> F. J. Iborra,<sup>3</sup> J. Ricardo Arias-González<sup>1,\*</sup> and Beatriz H. Juárez<sup>1,2,4,\*</sup>*

<sup>1</sup> IMDEA Nanoscience, Faraday 9, Campus de Cantoblanco, 28049, Madrid, Spain.

<sup>2</sup> Department of Applied Physical Chemistry. Universidad Autónoma de Madrid, 28049 Cantoblanco, Madrid, Spain

<sup>3</sup> National Center for Biotechnology (CNB-CSIC), Campus de Cantoblanco, 28049, Madrid, Spain.

<sup>4</sup> Condensed Matter Physics Center (IFIMAC), Universidad Autónoma de Madrid, 28049 Madrid, Spain.

## ABSTRACT

Laser tweezers afford quantum dot (QD) manipulation for its use as localized emitters. Here, we demonstrate fluorescence by radiative energy transfer from optically trapped colloidal QDs (donors) to fluorescent dyes (acceptors). To this end, we synthesized silica-coated QDs of different compositions and triggered their luminescence by simultaneous trapping and two-photon excitation in a microfluidic chamber filled with dyes. This strategy produces a near-field light source with great spatial maneuverability, which can be exploited to scan nanostructures. In this regard, we demonstrate induced photo-luminescence of dye-labelled cells *via* optically trapped silica-coated colloidal QDs placed at their vicinity. Allocating nanoscale donors at controlled distances from a

cell is an attractive concept in fluorescence microscopy because it dramatically reduces the number of excited dyes, which improves resolution by preventing interferences from the whole sample while prolonging dye luminescence lifetime due to the lower power absorbed from the QDs.

**KEYWORDS.** fluorescence microscopy, optical trapping, organic dye, quantum dot, radiative transfer, two-photon absorption.

Laser tweezers are a powerful tool to confine and manipulate small objects from micrometric to nanometric sizes down to the atomic level.<sup>1</sup> Recent applications in Materials Science and Biophysics include the study of gold nanoparticles,<sup>2</sup> nanorods,<sup>3,5</sup> globular proteins,<sup>6</sup> organelles,<sup>7</sup> polystyrene spheres with<sup>8</sup> and without emissive dyes,<sup>9</sup> colloidal quantum dots (QDs),<sup>10</sup> and magnetic nanoparticles,<sup>11</sup> to name a few. The versatility of this technique is not only due to its potential to exert and measure real-time force and torque in the nanoscale, but also because it offers a flexible combination with other methodologies. Localized light sources can couple to sub-wavelength structural elements, an idea that is exploited to break the resolution limit in near-field optics. In this regard, laser tweezers can optically confine nanostructures, thus allowing their spatial manipulation in real time.

The optical trapping of luminescent particles can be potentially used in biological imaging. The first approach to this application is to stimulate trapped particles using a secondary excitation beam.<sup>12</sup> However, if the trapping wavelength is carefully chosen, it is possible to simultaneously trap and excite luminescent probes with the same laser beam. For example, the non-linear response in alkaline niobate (XNbO<sub>3</sub>) nanowires,<sup>8,9</sup> and rare earth-based up-converting nanoparticles<sup>13,15</sup> can be triggered by tightly focusing of a continuous wave (CW) infrared laser under moderate power. In a similar fashion, optical trapping and excitation of QDs has been demonstrated under both CW<sup>16</sup> and pulsed near-infrared (NIR) laser irradiation<sup>17,18</sup> by a two-photon excitation (TPE) process.

The use of NIR CW-based optical trapping for TPE of QDs, requiring a smaller power density in the trap than pulsed excitation, has also been reported in recent years.<sup>10,16,19,20</sup> To reduce power losses due to tissue optical extinction, wavelengths within NIR biological windows are used.<sup>21</sup> This selective excitation, together with the combination of fluorophores in donor-acceptor configurations, allows the exploitation of energy transfer mechanisms. Particularly, the use of QD-dye as donor-acceptor pairs has been studied as a sensor for labelling, *in vitro* and *in vivo* imaging of cellular structures and diagnostics.<sup>22-27</sup> The observation of efficient non-radiative energy transfer, such as Förster Resonant Energy Transfer (FRET), typically implies donor-acceptor distances below 10 nm,<sup>38-40</sup> and fine control of the QD surface chemistry.<sup>24,41,42</sup> To record the luminescent signal from these experiments, imaging has been mainly performed by fluorescence microscopy.

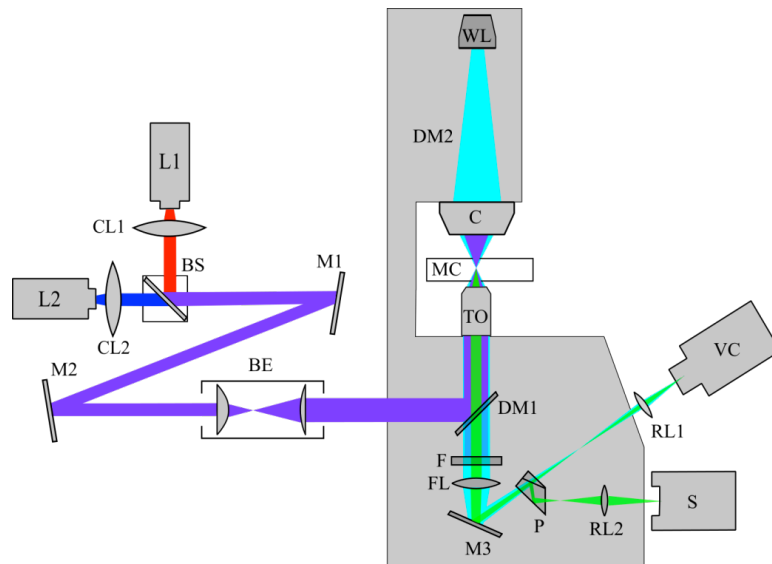
In this work, we propose an alternative approach to nanoscale imaging that excludes the need of an extended light source: we use an optical trap to control spatially the donor particles and study the optical excitation and photo-luminescence (PL) by reabsorption of organic dyes through the TPE of optically trapped QDs encapsulated in a SiO<sub>2</sub> shell, QDs@SiO<sub>2</sub>.<sup>43</sup> This shell inhibits FRET mechanisms. Under optimized conditions, including CW irradiation power in the first biological window, micrometric displacements to the detector and spectral overlap of QD@SiO<sub>2</sub>-donor and dye-acceptors controls the emission of dyes under low excitation intensity. Our results enable localized and spatially tuneable emission along micrometre ranges, which we herein apply to non-invasive cell imaging, a strategy that reduces dye photo-bleaching at long exposure times.

## RESULTS AND DISCUSSION

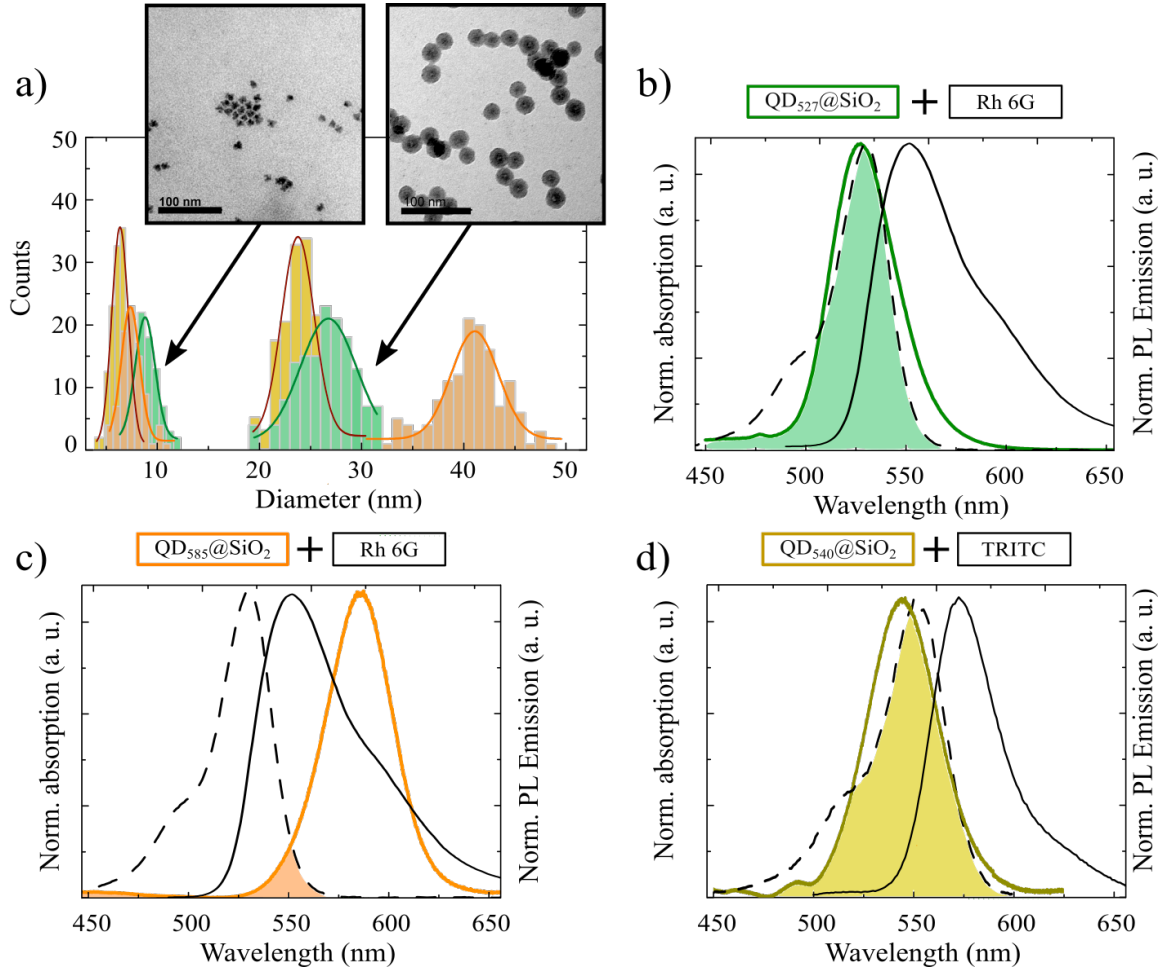
To study the radiative energy transfer process taking place between donor QDs@SiO<sub>2</sub> and acceptor dyes, a dual co-propagating-beam optical tweezers system as the one depicted in **Figure 1** was used (see experimental section for further details). Colloidal QDs consisted of CdSeZnS alloyed NCs with a CdS rich-core and a graded shell.<sup>43</sup> These

QDs have been encapsulated in SiO<sub>2</sub>, a strategy that reduces the cytotoxicity of mainly Cd-based colloidal QDs<sup>44-46</sup> at the cost of decreasing their photoluminescence quantum yield (PLQY). However, we reported that the right selection of capping ligands is key to retain the initial PLQY values.<sup>43</sup> Silica encapsulation, in addition, hinders Förster Resonance Energy Transfer (FRET), a well-known mechanism between donor and acceptors requiring distances typically smaller than 10 nm. The size distributions of the QDs and hybrid nanosystems used in this work (QD<sub>527</sub>@SiO<sub>2</sub>, QD<sub>540</sub>@SiO<sub>2</sub> and QD<sub>585</sub>@SiO<sub>2</sub>) are plotted in **Figure 2a**, where the subscripts account for the maximum PL wavelength. As an example, representative TEM images of QD<sub>527</sub> before and after SiO<sub>2</sub> encapsulation are displayed as insets. The size distributions show a SiO<sub>2</sub> shell with average thickness of (9.0 ± 2.9) nm for QD<sub>527</sub>@SiO<sub>2</sub>, (8.3 ± 1.3) nm for QD<sub>540</sub>@SiO<sub>2</sub> and of (16.9 ± 2.5) nm for QD<sub>585</sub>@SiO<sub>2</sub>.

To analyze the radiative energy transfer process taking place between donor QDs@SiO<sub>2</sub> and acceptor dyes, we have selected Rh6G and TRITC as dyes. **Figure 2b** shows the emission spectrum of the hybrid system QD<sub>527</sub>@SiO<sub>2</sub>. The PL maximum takes place at 527 nm, thus matching Rh6G maximum absorption around 530 nm, and the Rh6G in turn re-emits photons around 550 nm. The colored area shows the overlapping between the donor emission and the acceptor absorption. In contrast, QD<sub>585</sub>@SiO<sub>2</sub> emission hardly overlaps the Rh6G absorption, as depicted in **Figure 2c**. The longer emission wavelength for the smaller QD cores, see Figure 2a, is related to the specific composition of the QDs, as explained elsewhere.<sup>43</sup> The re-absorption efficiency of each donor-acceptor pair has been quantified by means of the overlapping integral in 6838 M<sup>-1</sup> cm<sup>-1</sup> for QD<sub>527</sub>@SiO<sub>2</sub>-Rh6G and 311 M<sup>-1</sup> cm<sup>-1</sup> for QD<sub>585</sub>@SiO<sub>2</sub>-Rh6G.<sup>47</sup> This means that radiative energy transfer in QD<sub>527</sub>@SiO<sub>2</sub>-Rh6G pairs is 22 times more effective than that of QD<sub>585</sub>@SiO<sub>2</sub>-Rh6G pairs. QD<sub>540</sub>@SiO<sub>2</sub>-TRITC pairs also present a significant spectral overlap, as shown in **Figure 2d**.

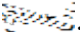


**Figure 1.** Combined optical trapping and fluorescence setup. Two lasers (L1 and L2, red and blue paths, respectively) are collimated (CL1 and CL2, collimation lenses, respectively) and combined using a polarizing beam splitter (BS). The combined beam (purple path) is directed into a fluorescence microscope by means of two mirrors (M1 and M2) and magnified with a beam expander (BE). A dichroic mirror (DM1) redirects the beams to the trapping objective (TO). Trapping experiments are performed inside a microfluidic chamber (MC). The PL from the optical trap focal region (green path) is collected by the TO, filtered from the stray laser light (F, fluorescence filter) and monitored (FL, focusing lens; M3, mirror; P, prism; RL1 and RL2, relay lenses) by a video camera (VC) and a spectrometer (S). The experiment is illuminated (blue path) by means of a halogen lamp (WL) and a low-NA condenser lens c).



**Figure 2.** Sample characterization. a) Size distributions of  $\text{QD}_{527}$ ,  $\text{QD}_{540}$  and  $\text{QD}_{585}$  cores (left group of histograms, green, yellow and orange, respectively) and silica-coated nanostructures,  $\text{QD}_{527}@\text{SiO}_2$ ,  $\text{QD}_{540}@\text{SiO}_2$  and  $\text{QD}_{585}@\text{SiO}_2$  (right group of histograms, green, yellow and orange, respectively), measured by TEM. Solid curves represent Gaussian fits to the experimental histograms yielding mean and standard deviations for the diameters of  $(8.8 \pm 1.9)$  nm,  $(6.48 \pm 0.04)$  nm,  $(7.4 \pm 2.0)$  nm,  $(26.7 \pm 5.5)$  nm,  $(23.1 \pm 1.0)$  nm and  $(41.1 \pm 4.6)$  nm, respectively. Left and right insets show TEM images of  $\text{QD}_{527}$  before and after silica encapsulation, respectively; scale bars, 100 nm. Spectroscopic behavior of the donor-acceptor pairs used in this work: b)  $\text{QD}_{527}@\text{SiO}_2$ -Rh 6G, c)  $\text{QD}_{585}@\text{SiO}_2$ -Rh 6G and d)  $\text{QD}_{540}@\text{SiO}_2$ -TRITC. In each case, the colored curve represents the normalized donor (QD) emission, the dash curve is the acceptor (Rh 6G or TRITC) normalized absorption and the black solid curve its normalized emission. The colored area shows the overlapping between the donor emission and the acceptor absorption.

## Behavior of the quantum dots in a low-intensity optical trap

To perform optical trapping experiments, QD@SiO<sub>2</sub> were dispersed in ethanol or water, where the nanoparticles form small aggregates or clusters, as characterized elsewhere.<sup>48</sup> The measured hydrodynamic diameter of the QD@SiO<sub>2</sub> aggregates was (0.95 ± 0.49) μm, and the number of nanoparticles contained in each cluster was estimated in .

### Energy transfer phenomenon

During optical trapping experiments, the lasers provide an average power of 90 mW in the spot corresponding to a flux of 2.8×10<sup>23</sup> photons/cm<sup>2</sup>·s (see experimental section for spot dimensions). Trapped QDs show PL through TPE as previously reported.<sup>10, 16, 19, 20, 48, 49</sup> Under the conditions reported here, Rh6G and TRITC dyes are not optically excited because our photon flux is deficient for TPE of organic dyes, generally requiring 10<sup>27</sup>-10<sup>29</sup> photons/cm<sup>2</sup>·s provided by pulsed sources at similar wavelengths.<sup>50, 51</sup>

As shown in **Figure 3a**, a trapped QD@SiO<sub>2</sub> system can be moved in the micrometer range within the chamber walls by means of a micrometer drive, hence making possible to evaluate the emitted PL throughout several thicknesses, *z*, of optically active medium. **Figure 3b** and **3c**, shows the modulated PL emission detected from the trap in a solution containing 2 μM Rh6G in ethanol for trapped QD<sub>527</sub>@SiO<sub>2</sub> and QD<sub>585</sub>@SiO<sub>2</sub>, respectively, in the counter-propagating laser setup. Approaching the trap to the collector system (minimum 20 μm) yields higher contribution of the QD<sub>527</sub>@SiO<sub>2</sub> emission and lower contribution of the dye emission, in good agreement with a lower quantity of dye molecules in the optical path. As the trap distance to the collector increases (up to 140 μm), the relative dye emission intensity also increases, in good agreement with an increased absorbing dye volume.



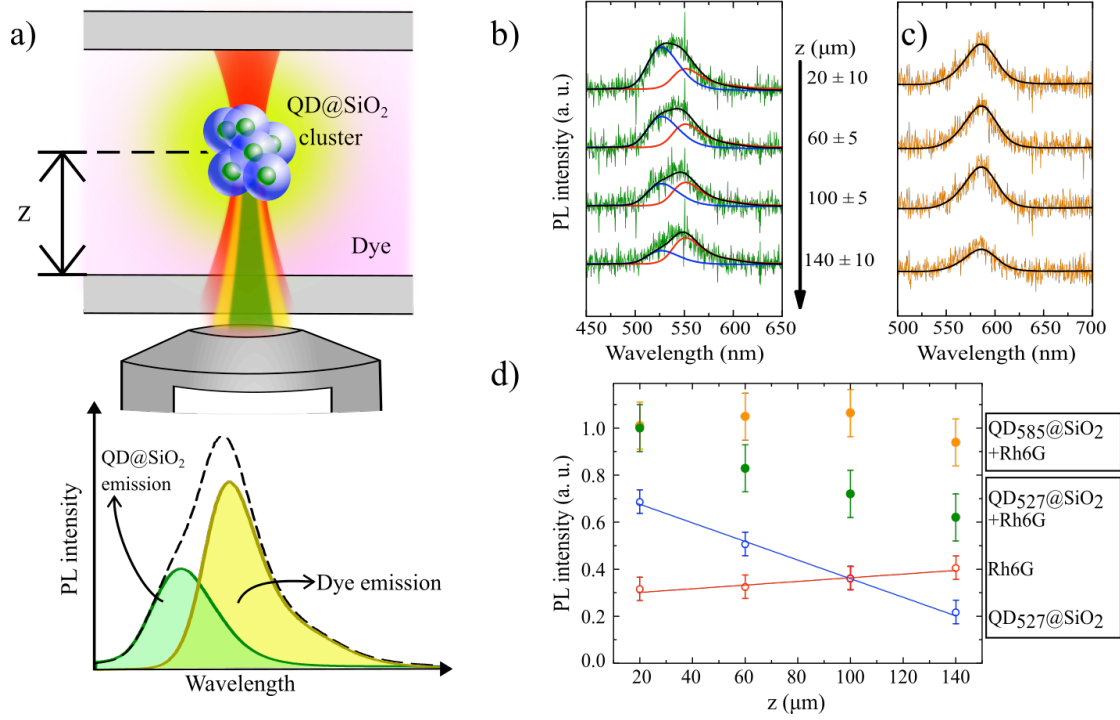


**Figure 3.** PL output dependence on the distance to the coverslip,  $z$ . *a)* Sketch of the experiment: Upper panel, an optically trapped QD@SiO<sub>2</sub> aggregate/cluster remains at a fixed position with respect to the collector objective while the microfluidics chamber is moved, as characterized by the distance between the optical trap and the front coverslip,  $z$ . A dye class, present in the dispersive medium at a certain concentration, re-absorbs the light emitted by the cluster. Lower panel, the emission spectrum collected by the trapping objective is a combination of the emission of the QD@SiO<sub>2</sub> cluster and the dye, whose relative contribution is given primarily by the dye concentration and the distance  $z$ . *b)* and *c)*, emission collected in the far field from an optically trapped QD cluster, QD<sub>527</sub>@SiO<sub>2</sub> or QD<sub>585</sub>@SiO<sub>2</sub>, respectively, in ethanol containing 2  $\mu\text{M}$  Rh6G, as a function of  $z$ . Black curve in *b)*, fitting of a linear superposition of the individual PL emissions from the QD<sub>527</sub>@SiO<sub>2</sub> (blue curve) and the Rh6G (red curve) according to Eq. (2). Black curve in *c)*, fitting of the individual emission from the QD<sub>585</sub>@SiO<sub>2</sub> measured in the fluorometer to the experimental data in the optical tweezers. *d)* Dependence of the PL intensity on the distance between the QD cluster and the front coverslip. Green dots represent the total PL collected signal when a QD<sub>527</sub>@SiO<sub>2</sub> cluster is in the trap; hollow blue and red dots, deconvoluted QD<sub>527</sub>@SiO<sub>2</sub> and Rh6G signals (note superposition at  $z=100$   $\mu\text{m}$ ). Linear fits are guides to the eye. Orange dots are the collected signals when a QD<sub>585</sub>@SiO<sub>2</sub> cluster is in the trap. Orange and green data are normalized by using Eq. (3) at  $z=20$   $\mu\text{m}$ .

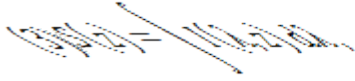
The spectral overlap between  $\text{QD}_{527}@\text{SiO}_2$  and Rh6G molecules (see Figure 2b) modifies donor far-field spectra by radiative energy transfer because a fraction of the photons emitted in the spectral overlapping region do not reach the collector.<sup>47</sup> Likewise, fluorescent far-field spectra lineshapes from the dyes are modified by energy homotransfer, which takes place among Rh6G molecules due to spectral overlapping of Rh6G absorption with its own emission.<sup>52</sup> Since both the fraction of photons emitted from the QDs that are re-absorbed by the dyes and the dye inner filter effect depend on acceptor concentration, these phenomena cause negligible distortions of both the  $\text{QD}@\text{SiO}_2$  and Rh6G far-field spectra for a low number of dye molecules in the solution. This is in fact what we observe in the experimental data of Figure 3b, where the overall collected spectrum can be approximated by the sum of the pure emissions from the  $\text{QDs}@\text{SiO}_2$  and the dyes (blue and red deconvoluted spectra in Figure 3b), respectively. More in depth, Figure 3b shows that the output emission lineshape measured in the optical tweezers setup,  $I(\lambda, z)$ , can be fitted to a linear superposition of the individual spectra of the  $\text{QD}_{527}@\text{SiO}_2$  and the Rh6G to a high quality:

$$I(\lambda, z) \approx A(z) \times I_{\text{QD}}(\lambda) + B(z) \times I_{\text{dye}}(\lambda), \quad (7)$$

where  $I_{\text{QD}}$  and  $I_{\text{dye}}$  are the intensity spectra obtained in bulk (ensemble-average) measurements in a fluorometer (for  $\text{QDs}@\text{SiO}_2$  and the dye, separately) and  $A(z)$  and  $B(z)$  are fitting parameters that account for the relative contribution of each emitter to the far-field signal.

The comparative experiment for  $\text{QDs}_{585}@\text{SiO}_2$  is shown in Figure 3c. In this case, a relatively constant PL emission spectrum is collected regardless of the distance from the trap to the collector system since inappreciable radiative energy transfer is taking place. Consequently, for this case of  $\text{QDs}_{585}@\text{SiO}_2$ , equation (2) reads  $I(\lambda) \approx I_{585}$ .

**Figure 3d** shows the total collected intensities for  $\text{QDs}@\text{SiO}_2$  in 2  $\mu\text{M}$  Rh6G in ethanol as a function of the distance  $z$ . In this graph, the total collected intensity of a trapped  $\text{QD}@\text{SiO}_2$  cluster in the presence of Rh6G has been normalized to the initial total intensity at  $z = 20 \mu\text{m}$ ,



so that their behavior, together with those from the deconvoluted signals  $I_{527}$  and  $I_{\text{Rh6G}}$ , with  $z$  can be compared. Again, in the presence of 2  $\mu\text{M}$  Rh6G the intensity does not depend on  $z$  for the  $\text{QD}_{585}@\text{SiO}_2$  system because of the small spectral overlap (orange dots, Figure 3d). The  $I(\lambda)$  decrease when the  $\text{QD}_{527}@\text{SiO}_2$  cluster separates from the coverslip (green dots) may be due to photodynamic bleaching.<sup>48</sup>

Deconvoluted signals for  $\text{QD}_{527}@\text{SiO}_2$  in a 2  $\mu\text{M}$  Rh6G ethanol solution show that the intensity from the  $\text{QD}_{527}@\text{SiO}_2$  component strongly attenuates also in the far field (hollow blue dots). On the other hand, the reemitted signal from the Rh6G component (hollow red dots) increases with the distance, which is expected due to the increasing number of dye molecules that fill the gap from the QD cluster to the coverslip as  $z$  grows. However, this growing trend with  $z$  is not very pronounced for a total concentration Rh6G 2  $\mu\text{M}$ , which almost saturates the overall collected far-field signal in the spectrometer. In relative terms, the Rh6G contribution to collected emission varies from 31% to 65% for distances between 20 and 140  $\mu\text{m}$  to the collector system, respectively. At 140  $\mu\text{m}$ , since only a small contribution of the  $\text{QD}_{527}@\text{SiO}_2$  is apparent, it can be concluded that at this distance the ratio donor-acceptor contribution is optimized for the given  $\text{QD}_{527}@\text{SiO}_2$ -dye pair concentration. Thus, micrometric control over the trap distance allows fine-tuning and optimization of the emission wavelength and intensity for either partial or practically total radiative energy transfer.

In order to extend our results to physiological media and improve fluorescence detection, we performed experiments using different concentrations of the dye tetramethylrhodamine (TRITC) in deionized water excited by the  $\text{QD}_{540}@\text{SiO}_2$  clusters in the co-propagating lasers setup. This dye has a PLQY around 0.28,<sup>53</sup> much lower than that of Rh6G, around 0.95.<sup>54</sup> For operational convenience, the experiments in this instrument were carried out from  $z=100$   $\mu\text{m}$  to the front surface, and consequently

results were normalized to the initial intensity at that distance according to Eq. (3). **Figure 4a**, top panel, shows the spectrum evolution when a trapped  $\text{QD}_{540}@\text{SiO}_2$  cluster is moved from  $z=100\ \mu\text{m}$  to  $z=10\ \mu\text{m}$  the front surface in a microfluidics channel filled by a  $6.25\ \mu\text{M}$  TRITC in deionized water. Because of the relatively high dye concentration in this trapping configuration, the TRITC emission dominates the collected spectrum, which remains unchanged within the entire  $z$  range, as shown in the corresponding lower panel. To detect changes in the emission lineshape, **Figure 4b**, top panel, TRITC concentration was lowered to  $12.2\ \text{nM}$ . As depicted in the bottom panel of this figure, TRITC contribution varies from almost 100% when the  $\text{QD}_{540}@\text{SiO}_2$  system is positioned at  $z=100\ \mu\text{m}$  to 88% when it is displaced to  $z=10\ \mu\text{m}$ . Contribution from  $\text{QD}_{540}@\text{SiO}_2$  becomes more apparent at even lower concentrations, as represented in **Figure 4c**, top panel, at  $2.7\ \text{nM}$  TRITC. In this case, TRITC relative intensity varies from 91% to 59% as the  $\text{QD}_{540}@\text{SiO}_2$  cluster is moved between  $z=100\ \mu\text{m}$  and  $z=10\ \mu\text{m}$ , as shown in the corresponding lower panel. Thus, not only the micrometric control over the trap distance allows optimization of the emission wavelength and intensity (as shown in Figure 3), but also the relative concentration of the dye for a given trapped QD system.

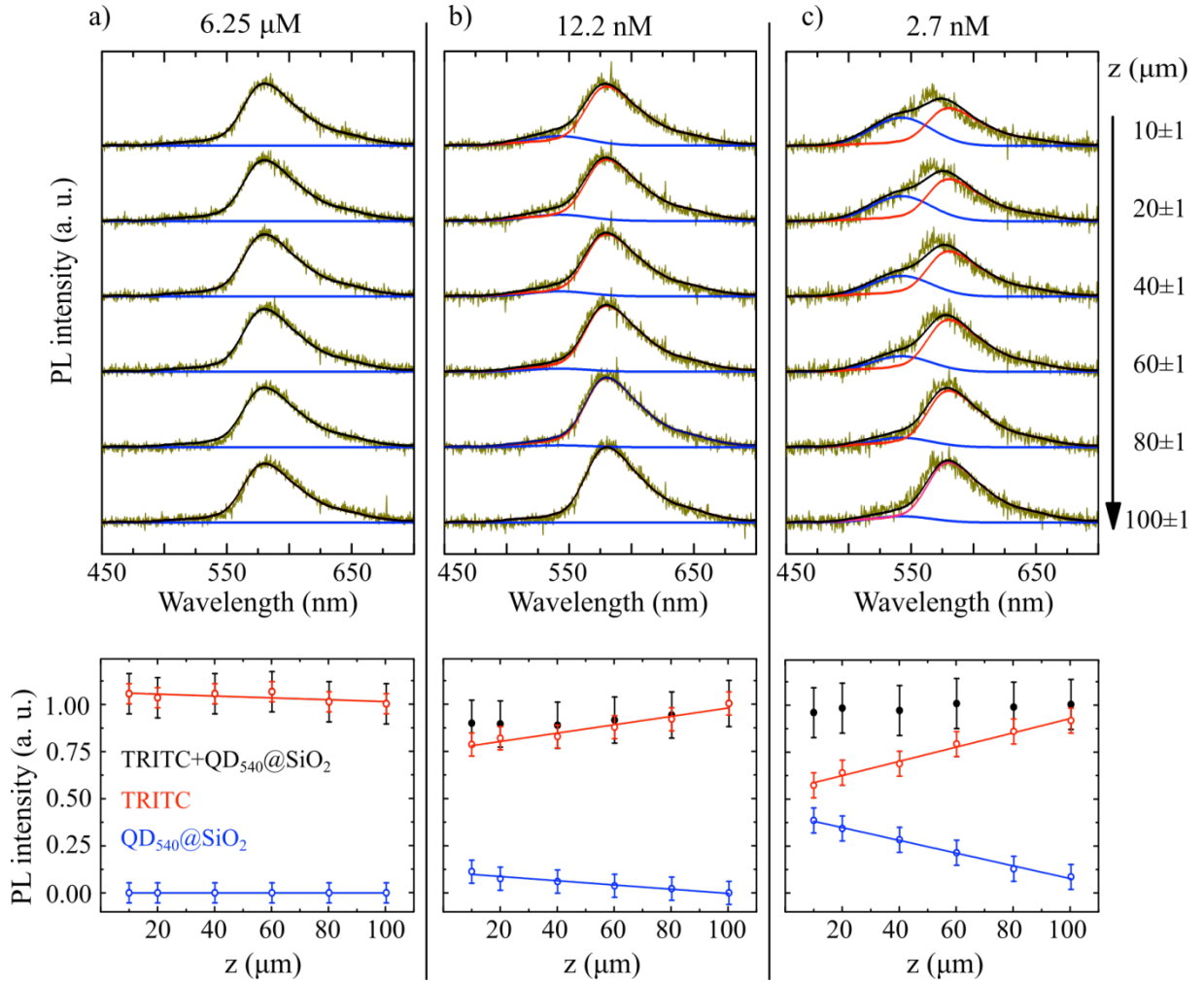


**Figure 4.** PL signal as a function of dye concentration. Top panels, emission collected in the far field from an optically trapped  $\text{QD}_{540}@SiO_2$  cluster in DI water containing a)  $6.25 \mu\text{M}$ , b)  $12.2 \text{ nM}$  and c)  $2.7 \text{ nM}$  of the dye TRITC as a function of  $z$ . Black curves, fitting of a linear superposition of the individual PL emissions from the  $\text{QD}_{540}@SiO_2$  (blue curves) and the TRITC (red curves) according to Eq. (2). Bottom panels, corresponding dependence of the PL intensity collected in the optical tweezers on the distance between the QD cluster and the front coverslip. Black dots represent the total collected signal when a  $\text{QD}_{540}@SiO_2$  cluster is in the trap; hollow blue and red dots correspond to deconvoluted  $\text{QD}_{540}@SiO_2$  and TRITC PL signals, respectively. Linear fits are guides to the eye. Black data are normalized by using Eq. (3) at  $z=100 \mu\text{m}$ .

### Excitation of dye-labeled cells

The aforementioned methodology can be followed to excite dye-labeled structures in a cell. In this case, the dye molecules are positioned within a cell instead of being dispersed in the medium. Jurkat-cells, whose proteins were nonspecifically labeled with Alexa Fluor 546 after membrane permeabilization, were used (see experimental). A

sketch of the experimental procedure is presented in **Figure 5**. Jurkat-cells were deposited on the bottom surface of the microfluidic chamber, where  $\text{QD}_{540}@\text{SiO}_2$  clusters were dispersed, trapped and moved around the Jurkat-cell area in order to obtain the emission from the labelled proteins. This system allows precise micrometer 3D position control of the  $\text{QD}_{540}@\text{SiO}_2$  system, which can be located anywhere around or above the Jurkat-cell, thus collecting luminescence from different zones.

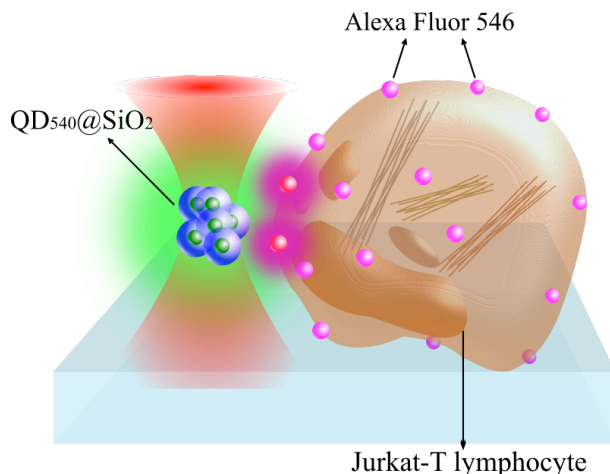


**Figure 5.** Sketch (not to scale) of the indirect excitation of a dye-labeled cell. A laser trapped  $\text{QD}_{540}@\text{SiO}_2$  cluster is positioned in the vicinity of a labelled Jurkat-cell with Alexa Fluor 546, immobilized on a glass substrate. PL emission from the trapped  $\text{QD}_{540}@\text{SiO}_2$  system excites the adjacent labelled structure. The PL emission from the trap and surrounding areas is collected through the trapping objective (not shown).

**Figure 6** shows the spectra collected from the trap and surrounding regions at several positions of the  $\text{QD}_{540}@\text{SiO}_2$  system with respect to the Jurkat-cell. When the  $\text{QD}_{540}@\text{SiO}_2$  system is trapped far ( $\sim 10 \mu\text{m}$ ) from the Jurkat-cell (Figure 6a), the emission lineshape equals that of  $\text{QD}_{540}@\text{SiO}_2$  in the spectrofluorometer. The same lineshape is collected even when the  $\text{QD}_{540}@\text{SiO}_2$  is approached to the Jurkat-cell up to a few microns (Figure 6b). A contribution from Alexa Fluor 546 is clearly observed when the  $\text{QD}_{540}@\text{SiO}_2$  cluster is in the vicinity of the Jurkat-cell membrane (Figure 6c). Interestingly, this contribution was appreciable when the particles were placed at distances comparable to the size of the laser focus, around  $1 \mu\text{m}$ . The  $\text{QD}@\text{SiO}_2$  system that was moved even closer to the cell membrane got irreversibly stuck to it. Furthermore, if the  $\text{QD}_{540}@\text{SiO}_2$  is trapped above the cell (*i.e.* focusing the trapping laser

and collecting the luminescence through the cell), Alexa Fluor 546 emission dominates the recorded signal, as shown in Figure 6d.

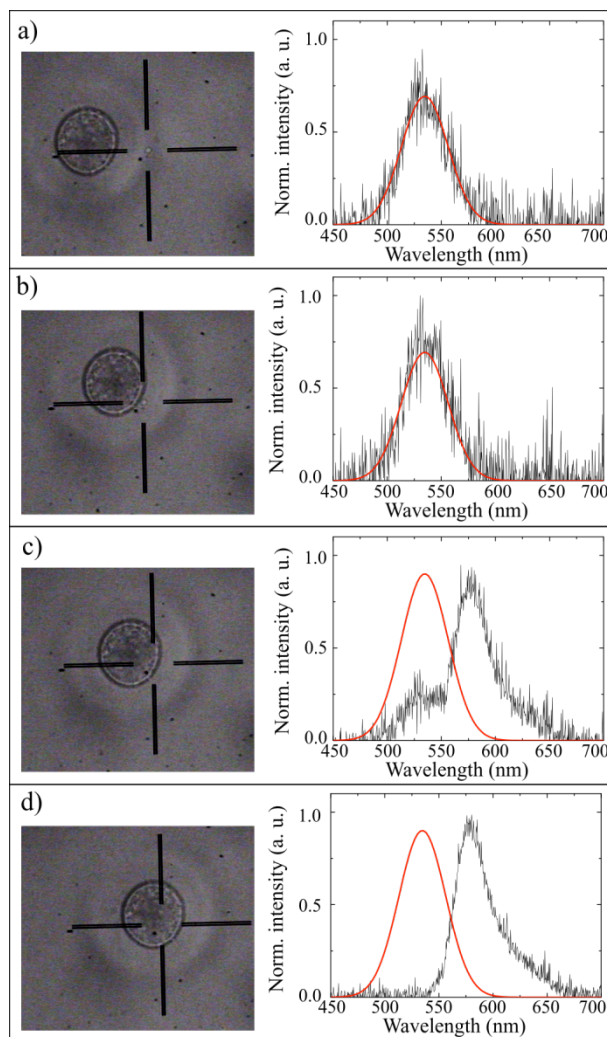


**Figure 6.** Emission spectra from labeled cells. Brightfield microscopy images and collected spectra (black curves) from a  $\text{QD}_{540}@\text{SiO}_2$  cluster trapped a)  $\sim 10 \mu\text{m}$  away from the Jurkat-cell, b) close (a few microns) to the labelled Jurkat-cell membrane, c) in the vicinity (within  $1\text{-}\mu\text{m}$ ) of the Jurkat-cell membrane and d) above the whole Jurkat-cell structure. The optical trap position roughly matches the reticle center. Red curves represent in all cases the emission of the original  $\text{QD}_{540}@\text{SiO}_2$ , as measured in a spectrofluorometer.

## CONCLUSIONS

We demonstrate PL of organic dye molecules through the optical trapping of silica-encapsulated QDs under CW excitation by means of two photon excitation and further radiative energy transfer. This reabsorption mechanism is clearly discernible at

relatively low dye concentrations. Our experiments evidence that, (i), the spectral overlap between QDs emission and dye absorption, (ii), the QD/dye relative concentration and, (iii), the influence of trap position in the collection of the far-field spectra allow a tunable final emission wavelength and intensity. An important feature of our approach to excite fluorescent molecules by optically trapped QDs is that the energy transfer phenomenon, despite its low efficiency, is so effective that fluorescence can be collected in the far-field at relatively low concentrations of the dye molecules. This versatile approach is useful for spectroscopy and imaging in biological environments with near-field selectivity, as supported by several facts: firstly, silica encapsulation discards resonant energy transfer, reduces cytotoxicity and allows experiments in aqueous media. Secondly, the use of CW near-infrared excitation sources limits biological damage. Finally, the low efficiency of this energy transfer promoting remotely controlled dye-emission prevents strong dye photobleaching effects thus enabling long-time experiments.

The spatial maneuverability of a point-like light source provided by optical tweezers offers an alternative to fluorescence imaging since it introduces the diffraction limit-breakage concept from near-field optics in live microscopy. In this regard, we envision a high potential for our results to increase resolution and non-invasiveness in live microscopy since it is still possible, on the one hand, to reduce the donor concentration down to one single luminescent nanoparticle in the trap and, on the other hand, to optimize collection optics to track signals from very low amounts of highly-localized dye molecules in a cell.

## **METHODS**

### **Synthesis and characterization of colloidal QDs**

The synthesis and further SiO<sub>2</sub>-coating of alloyed CdSeZnS QDs in microemulsion has been performed according to our previous report.<sup>43</sup> Three different QD samples have been used in this work, namely: QD<sub>527</sub>@SiO<sub>2</sub>, QD<sub>585</sub>@SiO<sub>2</sub> and QD<sub>540</sub>@SiO<sub>2</sub>, the first subscript corresponding to their wavelength photoluminescence (PL) maxima. Ethanol or



deionized water (Type 1 Ultrapure reagent grade water purification system; Wasserlab) dispersions of QD@SiO<sub>2</sub> have been sonicated before being flowed in a microfluidic chamber for the optical trapping experiments. Absorption and PL spectra were recorded in a Cary 50 spectrophotometer (Varian) and a spectrofluorometer (Horiba Jobin Yvon Fluoromax-4), respectively. QDs and QD@SiO<sub>2</sub> morphology were observed by transmission electron microscopy (TEM). Average size values were obtained from the TEM images, measuring at least 50 nanoparticles per sample.

### **Dye preparation**

For trapping experiments, 2  $\mu$ M solutions of rhodamine 6G (Rh6G) in ethanol from Sigma Aldrich (**R4127**) were prepared using aliquots from a 10  $\mu$ M stock solution. The Rh6G concentration was verified from the absorption coefficient measured in the spectrophotometer (Cary 50, Varian). A 0.05 mM stock solution of tetramethylrhodamine (TRITC) in deionized water was prepared and further diluted in the same way than the Rh6G solutions.

### **Optical tweezers setups**

A dual co-propagating-beam optical tweezers system was used (see **Figure 1**). In this setup, two 845-nm diode laser beams were combined into the same optical path by a NIR polarizing beam splitter. The resultant beam was focused by a microscope objective (Olympus UPLSApo, 60X; NA=1.2) inside a single-channel micro-fluidics chamber. This incident, combined beam overfills the objective back focal plane, thus using its total NA and increasing the trapping efficiency in this co-propagating configuration. The system was mounted in a commercial inverted fluorescence microscope (Zeiss Axiovert 135M). Luminescence from the optical trap was collected in reflection through the corresponding imaging camera port available in the microscope and analyzed by means of a spectrometer (Ocean Optics USB2000+).

Alternatively, some experiments were performed in a dual counter-propagating laser setup, wherein the size of the trapped particle can be elucidated by means of Thermal Noise Analysis or Stokes' test.<sup>55</sup> The beam waist diameter was estimated in 1.3  $\mu$ m. The

setup was modified in order to register the PL signal. Light generated in the trapping area is collected for analysis through one of the trapping objectives and redirected to a spectrometer (Ocean Optics USB2000+).

Home-made micro-fluidic chambers consisted of a NescoFilm (AZWELL, inc. Osaka, Japan) laser-imprinted channel sandwiched between two 0.1- $\mu\text{m}$  thick microscopy cover-slides. Channel width was about 150  $\mu\text{m}$  and slightly varied from chamber to chamber. The micro-fluidic chamber could be displaced between the objectives by a micrometric screw. By default, the optical trap was generated halfway between the coverslip walls in the micro-fluidic chamber, regardless of the setup.

### **Cell culture and labelling**

Jurkat T-cells cells were grown in RPMI medium (Gibco) supplemented with 10% fetal bovine serum (FBS, Hyclone) and penicillin-streptomycin (Sigma) in a 37°C humidified incubator with ~5% CO<sub>2</sub>. Global protein staining was carried out as follows: Jurkat cells were fixed with 4% Paraformaldehyde in PBS for 10 minutes at room temperature. Then, cells were permeabilized with 0.5% Triton X100 in PBS for 10 minutes at room temperature. The staining was performed by incubating permeabilized cells with Alexa Fluor 546 carboxylic acid, succinimidyl ester at 10 nM, which stains specifically amino groups in cellular proteins.

### **Cell probing studies**

T-cells were flowed in a microfluidic chamber and deposited on the bottom cover slip surface. QD<sub>540</sub>@SiO<sub>2</sub> clusters were dispersed in Ca<sup>2+</sup>-free PBS (from Sigma-Aldrich) and injected in the microfluidic chamber through a different dispenser tube for optical trapping experiments.

AUTHOR INFORMATION

**Corresponding Author**

[beatriz.hernandez@uam.es](mailto:beatriz.hernandez@uam.es), [beatriz.hernandez@imdea.org](mailto:beatriz.hernandez@imdea.org),  
[ricardo.ariasgonzalez@gmail.com](mailto:ricardo.ariasgonzalez@gmail.com)

## Present Addresses

†J. Ricardo Arias-González, present address: Optical Nanomanipulation Lab, Calle Londres, 44, 3ºD, 28028, Madrid, Spain.

## ACKNOWLEDGMENT

The authors thank A. Blanco and D. Granados for fruitful discussion and S. de Lorenzo for technical help.

H.R-R. is supported by an FPI-UAM 2015 fellowship (BES-2009-027909). M. A. thanks IMDEA Nanociencia for her contract. Authors acknowledge funding from the Spanish Ministry of Economy and Competitiveness through MAT2017-85617-R and Spanish Ministry of Science, Innovation and Universities RTI2018-101939-B-100. BHJ acknowledges financial support from the Spanish Ministry of Economy and Competitiveness, through the “Maria de Maeztu” (IFIMAC) and “Severo Ochoa” (IMDEA Nanoscience) Programmes for Units of Excellence in R&D.

## REFERENCES

1. Ashkin, A., Acceleration and Trapping of Particles by Radiation Pressure. *Phys. Rev. Lett.* **1970**, *24*, 156.
2. Hansen, P. M.; Bhatia, V. K.; Harrit, N.; Oddershede, L. B., Expanding the Optical Trapping Range of Gold Nanoparticles. *Nano Lett.* **2005**, *5*, 1937-1942.
3. Head, C. R.; Kammann, E.; Zanella, M.; Manna, L.; Lagoudakis, P. G., Spinning Nanorods – Active Optical Manipulation of Semiconductor Nanorods Using Polarised Light. *Nanoscale* **2012**, *4*, 3693-3693.

4. Pauzauskie, P. J.; Radenovic, A.; Trepagnier, E.; Shroff, H.; Yang, P.; Liphardt, J., Optical Trapping and Integration of Semiconductor Nanowire Assemblies in Water. *Nat. Mater.* **2006**, *5*, 97-101.
5. Selhuber-Unkel, C.; Zins, I.; Schubert, O.; Sönnichsen, C.; Oddershede, L. B., Quantitative Optical Trapping of Single Gold Nanorods. *Nano Lett.* **2008**, *8*, 2998-3003.
6. Pang, Y.; Gordon, R., Optical Trapping of a Single Protein. *Nano Lett.* **2012**, *12*, 402-406.
7. Hormeno, S.; Ibarra, B.; Chichon, F. J.; Habermann, K.; Lange, B. M.; Valpuesta, J. M.; Carrascosa, J. L.; Arias-Gonzalez, J. R., Single Centrosome Manipulation Reveals its Electric Charge and Associated Dynamic Structure. *Biophys. J.* **2009**, *97*, 1022-1030.
8. Nakayama, Y.; Pauzauskie, P. J.; Radenovic, A.; Onorato, R. M.; Saykally, R. J.; Liphardt, J.; Yang, P., Tunable Nanowire Nonlinear Optical Probe. *Nature* **2007**, *447*, 1098-1101.
9. Dutto, F.; Raillon, C.; Schenk, K.; Radenovic, a., Nonlinear Optical Response in Single Alkaline Niobate Nanowires. *Nano Lett.* **2011**, *11*, 2517-2521.
10. Jauffred, L.; Richardson, A. C.; Oddershede, L. B., Three-Dimensional Optical Control of Individual Quantum Dots. *Nano Lett.* **2008**, *8*, 3376-3380.
11. Rodríguez-Rodríguez, H.; de Lorenzo, S.; de la Cueva, L.; Salas, G.; Arias-Gonzalez, J. R., Optical Trapping of Single Nanostructures in a Weakly-Focused Beam. Application to Magnetic Nanoparticles. *J. Phys. Chem. C* **2018**, *112*, 18094-18101.
12. Reece, P. J.; Paiman, S.; Abdul-Nabi, O.; Gao, Q.; Gal, M.; Tan, H. H.; Jagadish, C., Combined Optical Trapping and Microphotoluminescence of Single InP Nanowires. *Appl. Phys. Lett.* **2009**, *95*, 101109-101109.

13. Haro-González, P.; del Rosal, B.; Maestro, L. M.; Rodríguez, E. M.; Naccache, R.; Capobianco, J. a.; Dholakia, K.; Solé, J. G.; Jaque, D., Optical Trapping of NaYF<sub>4</sub>:Er<sup>3+</sup>,Yb<sup>3+</sup> Upconverting Fluorescent Nanoparticles. *Nanoscale* **2013**, *5*, 12192-12199.
14. Mor, F. M.; Sienkiewicz, A.; Forró, L.; Jeney, S., Upconversion Particle as a Local Luminescent Brownian Probe: A Photonic Force Microscopy Study. *ACS Photonics* **2014**, *1*, 1251-1257.
15. Rodríguez-Sevilla, P.; Rodríguez-Rodríguez, H.; Pedroni, M.; Speghini, a.; Bettinelli, M.; Solé, J. G.; Jaque, D.; Haro-González, P., Assessing Single Upconverting Nanoparticle Luminescence by Optical Tweezers. *Nano Lett.* **2015**, *15*, 5068-5074.
16. Jauffred, L.; Oddershede, L. B., Two-Photon Quantum Dot Excitation during Optical Trapping. *Nano Lett.* **2010**, *10*, 1927-1930.
17. Chiang, W.-y.; Okuhata, T.; Usman, A.; Tamai, N.; Masuhara, H., Efficient Optical Trapping of CdTe Quantum Dots by Femtosecond Laser Pulses. *J. Phys. Chem. B* **2014**, *118*, 14010-14016.
18. Pan, L.; Ishikawa, A.; Tamai, N., Detection of Optical Trapping of CdTe Quantum Dots by Two-Photon-Induced Luminescence. *Phys. Rev. B* **2007**, *75*, 161305-161305.
19. Hormeño, S.; Bastús, N. G.; Juárez, B. H.; Pietsch, A.; Weller, H.; Arias-Gonzalez, J. R., Plasmon-Exciton Interactions on Single Thermoresponsive Platforms Demonstrated by Optical Tweezers. *Nano Lett.* **2011**, *11*, 4742-4747.
20. Jauffred, L.; Kyrsting, A.; Arnspang, E. C.; Reihani, S. N. S.; Oddershede, L. B., Sub-Diffraction Positioning of a Two-Photon Excited and Optically Trapped Quantum Dot. *Nanoscale* **2014**, *6*, 6997-7003.
21. Smith, A. M.; Mancini, M. C.; Nie, S., Bioimaging: Second Window for *In Vivo* Imaging. *Nat. Nanotechnol.* **2009**, *4*, 710-711.

22. Bakalova, R.; Zhelev, Z.; Ohba, H.; Baba, Y., Quantum Dot-Conjugated Hybridization Probes for Preliminary Screening of siRNA Sequences. *J. Am. Chem. Soc.* **2005**, *127*, 11328-11335.
23. Chen, G.; Song, F.; Xiong, X.; Peng, X., Fluorescent Nanosensors Based on Fluorescence Resonance Energy Transfer (FRET). *Ind. Eng. Chem. Res.* **2013**, *52*, 11228-11245.
24. Gill, R.; Willner, I.; Shweky, I.; Banin, U., Fluorescence Resonance Energy Transfer in CdSe/ZnS–DNA Conjugates: Probing Hybridization and DNA Cleavage. *J. Phys. Chem. B* **2005**, *109*, 23715-23719.
25. Rowland, C. E.; Susumu, K.; Stewart, M. H.; Field, L. D.; Sangtani, A.; L., M. I.; Delehanty, J. B., Cellular Applications of Semiconductor Quantum Dots at the U.S. Naval Research Laboratory: 2006-2016. *Rev. Fluoresc.* **2016**, *2017*, 203-242.
26. Hildebrandt, N.; Spillmann, C. M.; Algar, W. R.; Pons, T.; Stewart, M. H.; Oh, E.; Susumu, K.; D. 'az , S. A.; Delehanty, J. B.; Medintz, I. L., Energy Transfer with Semiconductor Quantum Dot Bioconjugates: A Versatile Platform for Biosensing, Energy Harvesting, and Other Developing Applications. *Chem. Rev.* **2017**, *117*, 536--711.
27. Clapp, A. R.; Medintz, I. L.; Mauro, J. M.; Fisher, B. R.; Bawendi, M. G.; Mattoussi, H., Fluorescence Resonance Energy Transfer Between Quantum Dot Donors and Dye-Labeled Protein Acceptors Förster Resonance Energy Transfer. *J. Am. Chem. Soc.* **2004**, *126*, 301-310.
28. Tran, P. T.; Anderson, G. P.; Mauro, J. M.; Mattoussi, H., Use of Luminescent CdSe–ZnS Nanocrystal Bioconjugates in Quantum Dot-Based Nanosensors. *Phys Status Solidi B* **2002**, *229*, 427--432.

29. Medintz, I. L.; Clapp, A. R.; Mattoussi, H.; Goldman, E. R.; Fisher, B.; Mauro, J. M., Self-Assembled Nanoscale Biosensors Based on Quantum Dot FRET Donors. *Nat. Mater.* **2003**, *2*, 630.
30. Kim, J. H.; Morikis, D.; Ozkan, M., Adaptation of Inorganic Quantum Dots for Stable Molecular Beacons. *Sens. Actuator B-Chemical* **2004**, *102*, 315--319.
31. Lemon, C. M.; Karnas, E.; Han, X.; Bruns, O. T.; Kempa, T. J.; Fukumura, D.; Bawendi, M. G.; Jain, R. K.; Duda, D. G.; Nocera, D. G., Micelle-Encapsulated Quantum Dot-Porphyrin Assemblies as in Vivo Two-Photon Oxygen Sensors. *J. Am. Chem. Soc.* **2015**, *137*, 9832--9842.
32. Levy, M.; Cater, S. F.; Ellington, A. D., Quantum-Dot Aptamer Beacons for the Detection of Proteins. *ChemBioChem* **2005**, *6*, 2163--2166.
33. Drozdek, S.; Szeremeta, J.; Lamch, L.; Nyk, M.; Samoc, M.; Wilk, K. A., Two-Photon Induced Fluorescence Energy Transfer in Polymeric Nanocapsules Containing CdSexS1-x/ZnS Core/Shell Quantum Dots and Zinc (II) Phthalocyanine. *J. Phys. Chem. C* **2016**, *120*, 15460--15470.
34. Jung, S. a. C. X., Quantum Dot-Dye Conjugates for Biosensing, Imaging, and Therapy. *Adv. Healthcare Mater.* **2018**, *7*, 1800252.
35. Grecco, H. E.; Lidke, K. A.; Heintzmann, R.; Lidke, D. S.; Spagnuolo, C.; Martinez, O. E.; Jares-Erijman, E. A.; Jovin, T. M., Ensemble and Single Particle Photophysical Properties (Two-Photon Excitation, Anisotropy, FRET, Lifetime, Spectral Conversion) of Commercial Quantum Dots in Solution and in Live Cells. *Microsc. Res. Tech.* **2004**, *65*, 169-179.
36. Nag, O. K.; Stewart, M. H.; Deschamps, J. R.; Susumu, K.; Oh, E.; Tsytsarev, V.; Tang, Q.; Efros, A. L.; Vaxenburg, R.; Black, B. J.; Chen, Y.; O'Shaughnessy, T. J.; North, S. H.; Field, L. D.; Dawson, P. E.; Pancrazio, J. J.; Medintz, I. L.; Chen, Y.; Erzurumlu, R. S. Huston, A. L. et al, Quantum Dot-Peptide-Fullerene Bioconjugates

for Visualization of in Vitro and in Vivo Cellular Membrane Potential. *ACS Nano* **2017**, *11*, 5598-5613.

37. Patolsky, F.; Gill, R.; Weizmann, Y.; Mokari, T.; Banin, U.; Willner, I., Lighting-Up the Dynamics of Telomerization and DNA Replication by CdSe–ZnS Quantum Dots. *J. Am. Chem. Soc.* **2003**, *125*, 13918-13919.

38. Beane, G.; Boldt, K.; Kirkwood, N.; Mulvaney, P., Energy Transfer Between Quantum Dots and Conjugated Dye Molecules. *J. Phys. Chem. C* **2014**, *118*, 18079-18086.

39. Dworak, L.; Matylitsky, V. V.; Ren, T.; Basché, T.; Wachtveitl, J., Acceptor Concentration Dependence of Förster Resonance Energy Transfer Dynamics in Dye-Quantum Dot Complexes. *J. Phys. Chem. C* **2014**, *118*, 4396-4402.

40. Kowerko, D.; Schuster, J.; Amecke, N.; Abdel-Mottaleb, M.; Dobraza, R.; Würthner, F.; von Borczyskowski, C., FRET and Ligand Related Non-FRET Processes in Single Quantum Dot-Perylene Bisimide Assemblies. *Phys. Chem. Chem. Phys.* **2010**, *12*, 4112-4123.

41. Clapp, A. R.; Medintz, I. L.; Mattoussi, H., Förster Resonance Energy Transfer Investigations Using Quantum-Dot Fluorophores. *ChemPhysChem* **2006**, *7*, 47-57.

42. Liu, X.; Freeman, R.; Golub, E.; Willner, I., Chemiluminescence and Chemiluminescence Resonance Energy Transfer (CRET) Aptamer Sensors Using Catalytic Hemin/G-Quadruplexes. *ACS Nano* **2011**, *5*, 7648-7655.

43. Acebrón, M. a.; Galisteo-López, J. F.; Granados, D.; López-Ogalla, J.; Gallego, J. M.; Otero, R.; López, C.; Juárez, B. H., Protective Ligand Shells for Luminescent SiO<sub>2</sub>-Coated Alloyed Semiconductor Nanocrystals. *ACS Appl. Mater. Interfaces* **2015**, *7*, 6935-6945.



44. Aubert, T.; Soenen, S. J.; Wassmuth, D.; Cirillo, M.; Van Deun, R.; Braeckmans, K.; Hens, Z., Bright and Stable CdSe/CdS@SiO<sub>2</sub> Nanoparticles Suitable for Long-Term Cell Labeling. *ACS Appl. Mater. Interfaces* **2014**, *6*, 11714-11723.
45. Bruchez, M., Jr.; Moronne, M.; Gin, P.; Weiss, S.; Alivisatos, A. P., Semiconductor Nanocrystals as Fluorescent Biological Labels. *Science* **1998**, *281*, 2013-2016.
46. Gerion, D.; Pinaud, F.; Williams, S. C.; Parak, W. J.; Zanchet, D.; Weiss, S.; Alivisatos, A. P., Synthesis and Properties of Biocompatible Water-Soluble Silica-Coated CdSe/ZnS Semiconductor Quantum Dots. *J. Phys. Chem. B* **2001**, *105*, 8861-8871.
47. Valeur, B., *Molecular Fluorescence*. 2001; Vol. 8, p 402.
48. Rodriguez-Rodriguez, H.; Acebron, M.; Juarez, B. H.; Arias-Gonzalez, J. R., Luminescence Dynamics of Silica-Encapsulated Quantum Dots During Optical Trapping. *J. Phys. Chem. C* **2017**, *121*, 10124-10130.
49. Jensen, R.; Huang, I.-C.; Chen, O.; Choy, J. T.; Bischof, T. S.; Loncar, M.; Bawendi, M. G., Optical Trapping and Two-Photon Excitation of Colloidal Quantum Dots using Bowtie Apertures. *ACS Photonics* **2016**, *3*, 423-427.
50. Fischer, a.; Cremer, C.; Stelzer, E. H., Fluorescence of Coumarins and Xanthenes after Two-Photon Absorption with a Pulsed Titanium-Sapphire Laser. *Appl. Opt.* **1995**, *34*, 1989-2003.
51. Xu, C.; Webb, W. W., Measurement of Two-Photon Excitation Cross Sections of Molecular Fluorophores with Data from 690 to 1050 nm. *J. Opt. Soc. Am. B* **1996**, *13*, 481-491.
52. Fonin, A. V.; Sulatskaya, A. I.; Kuznetsova, I. M.; Turoverov, K. K., Fluorescence of Dyes in Solutions with High Absorbance. Inner Filter Effect Correction. *PLoS ONE* **2014**, *9*, e103878.

53. Haugland, R. P., Covalent Fluorescent Probes. **1983**, 29--58.

54. Magde, D.; Wong, R.; Seybold, P. G., Fluorescence Quantum Yields and their Relation to Lifetimes of Rhodamine 6G and Fluorescein in Nine Solvents: Improved Absolute Standards for Quantum Yields. *Photochem. Photobiol.* **2002**, *75*, 327-334.

55. Smith, S. B.; Cui, Y.; Bustamante, C., Optical-trap force transducer that operates by direct measurement of light momentum. *Methods Enzymol.* **2003**, *361*, 134-162.

TOC

